

**Molecular Characterization of Alkyl Nitrates in Atmospheric Aerosols
by Ion Mobility Mass Spectrometry**

Xuan Zhang^{1,*}, Haofei Zhang^{2,3}, Wen Xu⁴, Geoffrey S. Tyndall¹, John J. Orlando¹,
John T. Jayne⁴, Douglas R. Worsnop⁴, and Manjula R. Canagaratna^{4,*}

¹ Atmospheric Chemistry Observation & Modeling Laboratory, National Center for Atmospheric Research, Boulder, CO 80301, USA

² Department of Chemistry, University of California, Riverside, CA 92521, USA

³ Environmental Toxicology Program, University of California, Riverside, CA 92521, USA

⁴ Center for Aerosol and Cloud Chemistry, Aerodyne Research Inc., Billerica, MA 01821, USA

Correspondence to: Xuan Zhang (xuanz@ucar.edu)

Manjula R. Canagaratna (mrcana@aerodyne.com)

Abstract

We demonstrate the capability of the Ion Mobility Mass Spectrometry (IMS-MS) for molecular characterization of reactive and short-lived alkyl nitrates (ANs) in atmospheric aerosols. We show significantly enhanced sensitivity towards the intact molecules of ANs by ultimately two orders of magnitude with the addition of inorganic anions such as chloride and nitrate to the negative electrospray to promote the ion adduct formation. This approach enables the measurement of ANs that have low tendency to form molecular ions on their own with improved limit of detection in the range of 0.1 to 4.3 μM . Molecular identities of the ANs are well constrained by the developed collision cross section vs. mass to charge ratio correlation, which provides a two-dimensional separation of the $-\text{ONO}_2$ containing compounds on the basis of their molecular size and geometry. Structural information of the nitrate molecules is further probed by the identification of characteristic fragments produced from the collision induced dissociation of parent AN adducts. Application of the IMS-MS technique is exemplified by the identification of hydroxy nitrates in secondary organic aerosols produced from the photochemical oxidation of isoprene.

1. Introduction

Alkyl nitrates (ANs; $\text{ANs} = \text{RONO}_2$) constitute a major fraction and serve as a temporary reservoir of total reactive nitrogen oxides in the atmosphere (Perring et al., 2013). ANs are primarily produced from the hydroxyl radical (OH) initiated oxidation of volatile organic compounds (VOCs) in the presence of nitrogen oxides (NO_x) during daytime and the nitrate radical (NO_3) initiated oxidation of alkenes during nighttime. Once formed, ANs are primarily subjected to further chemical transformation leading to the recycling of NO_x , partitioning into the particle phase forming secondary organic aerosols (SOA), or deposition resulting in the loss of atmospheric NO_x . Characterization of alkyl nitrates is of crucial importance in understanding regional NO_x budget, tropospheric ozone production, as well as chemical mechanisms leading to the SOA formation (Brown et al., 2009; Farmer et al., 2011; Rollins et al., 2012; Rosen et al., 2004).

A suite of analytical techniques, such as thermal dissociation laser-induced-fluorescence spectroscopy (TD-LIF) (Thornton et al., 2000; Day et al., 2002; Wooldridge et al., 2010), chemical ionization mass spectrometry (CIMS) (Beaver et al., 2012; Loza et al., 2014; Krechmer et al., 2015; Nguyen et al., 2015; Schwantes et al., 2015; Teng et al., 2015; Xiong et al., 2015; Schwantes et al., 2017b; Lambe et al., 2017), and gas chromatography coupled with electron capture detection (GC-ECD) (Atlas, 1988; O'Brien et al., 1995; He et al., 2011), have been employed for *in situ* measurement of total and individual ANs in the gas phase. Observations of ANs in the particle phase, however, are rather limited due to the intensive denitrification during the preparation and analysis of particle samples. Efforts have been made to characterize the total amount of ANs and the number of $-\text{ONO}_2$ functional groups using TD-LIF and Fourier transform infrared spectroscopy (FTIR) (Rollins et al., 2010; Russell et al., 2011). The $\text{NO}_2^+ / \text{NO}^+$ ratio derived from the aerosol mass spectrometry (AMS) measurements has also been used as an indicator for the presence of alkyl nitrates in submicrometer particles (Farmer et al., 2010; Kiendler-Scharr et al., 2016; Xu et al., 2017; Xu et al., 2018). These techniques have provided important insights into the prevalence and abundance of ANs in atmospheric aerosols, although the molecular information of individual ANs is lacking. Recent development on the filter inlet for gases and aerosols (FIGAERO) interfaced with the CIMS instrument has allowed for on-line speciation and quantification of functionalized alkyl nitrates in the particle phase (Lee et al., 2016). While the molecular composition of any given compounds can be inferred from the mass spectra, structural

information on isomeric and isobaric species that are commonly produced from atmospheric chemical transformation is not available from CIMS measurements.

In this study, we present the first demonstration of the Ion Mobility Mass Spectrometry (IMS-MS) interfaced with an Electrospray Ionization (ESI) source that enables the molecular characterization of alkyl nitrates in atmospheric aerosols. The IMS technique has been widely employed in the fields of biochemistry and homeland security. The majority of previous studies that adapted ESI for IMS analysis employed either the Desorption Electrospray Ionization (DESI) to detect trace amounts of ANs on ambient surfaces (Cotte-Rodríguez et al., 2005; Popov et al., 2005; Takáts et al., 2005; Justes et al., 2007) or the Secondary Electrospray Ionization (SESI) for gas-phase ANs measurements (Tam and Hill, 2004; Martínez-Lozano et al., 2009; Crawford and Hill, 2013). The analysis of ANs directly from liquid solutions, on the other hand, has not yet been widely explored. Hilton et al. (2010) found that the NO_3^- fragment dominates the IMS spectra of several types of ANs measured in the negative ESI, suggesting these nitrate molecules readily fragment due to the thermally labile nature of the $-\text{ONO}_2$ functionality, thereby resulting in the loss of molecular information of the targeted compounds. Here we show that with the addition of selected anions including chloride, nitrate, iodide, and acetate into the sprayed solution, molecular structures of ANs are largely maintained by producing ion clusters of the form $[\text{M}+\text{Cl}]^-$, $[\text{M}+\text{NO}_3]^-$, $[\text{M}+\text{I}]^-$, and $[\text{M}+\text{Ac}]^-$, respectively. The anion attachment represents a new option for the detection of the $-\text{ONO}_2$ functionality that is unlikely to produce measurable amount of molecular ions on its own during ESI. The optimal anion concentration to essentially promote the ion adduct formation is on the order of milli-molar, which is significantly higher than the level of those naturally present in ambient aerosols. We develop an intrinsic collision cross section vs. mass to charge ratio correlation based on the ion mobility measurements of five AN standards, providing a two-dimensional identification of unknown molecules that are likely containing the $-\text{ONO}_2$ moiety. Additionally, the molecular identity of ANs can be verified via the characteristic fragment produced from the collision induced dissociation of the parent ion adducts. We apply the IMS-MS technique to identify ANs in SOA produced from isoprene photochemistry.

2. Experiments

2.1. Materials

Organic nitrate and nitro standards stored in acetonitrile ampules, including 1-mononitroglycerin (100 $\mu\text{g/mL}$, SigmaAldrich), 1,3-dinitroglycerin (100 $\mu\text{g/mL}$,

SigmaAldrich), pentaerythritol tetranitrate (1000 $\mu\text{g/mL}$, SigmaAldrich), hexahydro-1,3,5-trinitro-1,3,5-triazine (1000 $\mu\text{g/mL}$, SigmaAldrich), and 2,4-dinitrotoluene (1000 $\mu\text{g/mL}$, SigmaAldrich), were further diluted with methanol (HPLC grade, J. T. Baker) to 5 μM or less for characterizing the performance of the Ion Mobility Mass Spectrometer. Stock solutions of ammonium acetate (>99%, SigmaAldrich), ammonium chloride (>99%, SigmaAldrich), sodium nitrate (>99%, SigmaAldrich), and sodium iodide (>99%, SigmaAldrich) were prepared at a concentration of 10 mM in methanol. They were used as additives at typical concentrations of 0.01 – 0.1 mM in the ANs methanol solutions to promote the ion adducts formation.

2.2. Experiments

SOA samples containing alkyl nitrates were generated from the OH-oxidation of isoprene under high- NO_x conditions in the NCAR 10 m^3 Atmospheric Simulation Chamber (Zhang et al., 2018). H_2O_2 was used as the OH source by evaporating 133 μL aqueous solution (30 wt% in water, SigmaAldrich) into the chamber with 5 L/min purified air for ~ 120 min, resulting in a starting concentration of ~ 4 ppm (Wang et al., 2009; He et al., 2010; Zhao et al., 2011; Cappa et al., 2013; Zhang and Seinfeld, 2013; Schwantes et al., 2017a). Isoprene was injected into the chamber by evaporating ~ 17 μL liquid standard ($\geq 99\%$, SigmaAldrich) with 5 L/min purified air for ~ 20 min, resulting an initial concentration of ~ 500 ppb. NO was injected into the chamber from a concentrated NO cylinder source ($\text{NO} = 133.16$ ppm, balance N_2) to achieve an initial concentration of ~ 500 ppb. Seed aerosol was injected into the chamber by atomizing 0.06 M aqueous ammonium sulfate solution to provide sufficient surface area for the partitioning of alkyl nitrates (Nguyen et al., 2014a; Nguyen et al., 2014b; Zhang et al., 2014a; Zhang et al., 2015b; McVay et al., 2016; Nah et al., 2016; Huang et al., 2018). The chamber contents were allowed to mix for ~ 30 min before the onset of irradiation. After ~ 2 hr photooxidation, NO was nearly depleted (> 5 ppb) and the irradiation was ceased. SOA produced was then collected on Teflon filters (47-mm diameter, 0.5- μm pore size, MILLIPORE) through active sampling at a flow rate of 10 L/min for ~ 3 hr (Schilling Fahnstock et al., 2014; Zhang et al., 2014b; Huang et al., 2016; Thomas et al., 2016). Filters were stored in a -20 $^\circ\text{C}$ freezer prior to analysis (Riva et al., 2016). SOA samples were extracted in 20 mL HPLC-grade methanol by 45 min of sonication at ~ 273 K and then concentrated to ~ 5 mL with the assistance of a ~ 2 L/min N_2 stream.

2.3. Instrumental

The Electrospray Ionization Drift-Tube Ion Mobility Spectrometer (DT-IMS) interfaced to a Time-of-Flight Mass Spectrometer (TOFMS) was utilized in the characterization of ANs. The instrument was designed and manufactured by ToFwerk (AG, Switzerland), with detailed descriptions and schematics provided by previous studies (Kaplan et al., 2010; Groessl et al., 2015; Krechmer et al., 2016; Zhang et al., 2016b; Zhang et al., 2017). Here we will present the instrument operation protocols specific to the ANs measurement.

AN standards and SOA filter extracts were delivered to the ESI source via a 250 μL gas-tight syringe (Hamilton) held on a syringe pump (Harvard Apparatus) at a flow rate of 1 $\mu\text{L min}^{-1}$. The optimal ESI potential to readily generate stable ion adducts while minimizing the corona discharge was found to be -1800 V . The negatively charged mist generated at the emitter tip is introduced into the drift tube through a Bradbury-Nielson ion gate located at the entrance with the assistance of 1 L min^{-1} nitrogen sheath gas. The BN ion gate was operated at the Hadamard Transform mode, with a closure voltage of 50 V and a gate pulse frequency of $1.2 \times 10^3\text{ Hz}$. The drift tube was held at a constant temperature ($340 \pm 3\text{ K}$) and atmospheric pressure ($\sim 766\text{ Torr}$). A counter flow of N_2 drift gas was introduced at the end of the drift region at a flow rate of 1.2 mL min^{-1} . Ion mobility separation was carried out at the field strength ranging from 300 to 400 V cm^{-1} . After exiting from the drift tube, ions were focused into a pressure-vacuum interface that includes two segmented quadrupoles (Q_1 and Q_2) through an ion lens and a nozzle. Note that the potential gradient applied to the ion lens and nozzle should be limited to 500 V or less to prevent intensive fragmentation of the molecular ions. The frequency and amplitude were set as $1.5 \times 10^6\text{ Hz}$ and 196 V for Q_1 and $1.5 \times 10^6\text{ Hz}$ and 250 V for Q_2 , respectively. Collision induced dissociation (CID) can be performed by adjusting the voltages on the ion optical elements between the two quadrupole stages. Over the course of a CID program, the quadrupoles were set to $1.3 \times 10^6\text{ Hz}$ and 120 V for Q_1 and $1.2 \times 10^6\text{ Hz}$ and 150 V for Q_2 , respectively, to ensure good transmission of low masses ($m/z < 100$).

The ESI-IMS-TOFMS instrument was operated in the m/z range of 20 to 1500 with a total recording time of 60 s for each dataset. The mass spectrometer was calibrated using sodium nitrate, ammonium phosphate, sodium dodecyl sulfate, sodium taurocholate hydrate, and ultramark 1621 in the negative mode. The ion mobility measurements were calibrated using tetrabutyl ammonium chloride as the instrument standard and 2,4-lutidine as the mobility standard (Zhang et al., 2016b). The average IMS (t/dt_{50}) and MS

(m/dm_{50}) resolving powers are ~ 80 and ~ 4000 , respectively. Mass spectra and ion mobility spectra were collected by Aquility DAQ v2.1.0 and post processed by Tofware v2.5.3.

3. Results and Discussion

3.1. Ion adduct formation

The strong electron affinity of the $-\text{ONO}_2$ functional group makes alkyl nitrate a potential candidate for being analyzed in the negative electrospray ionization mode. However, the ESI(−) mass spectra of the AN standards investigated here are typically characterized by various fragments and clusters due principally to the thermally labile $-\text{ONO}_2$ moiety. As shown in Figure 1, no molecular ion ($[\text{M}]^-$ or $[\text{M-H}]^-$) is observed on the ESI(−) mass spectra of 1-mononitroglycerin (MNG), 1,3-dinitroglycerin (DNG), and pentaerythritol tetranitrate (PETN). Instead, a small peak appears as a cluster ion of the form $[\text{M}+\text{NO}_2-\text{H}]^-$. It is worth noting that addition of water to the mobile phase does not promote the molecular ion formation, rather significant nitrate losses via hydrolysis were observed. With the addition of trace amount of salts, i.e., ammonium chloride (NH_4Cl), sodium nitrate (NaNO_3), sodium iodide (NaI), and ammonium acetate (NH_4Ac), the overall signal intensities were significantly enhanced through the production of a suite of adduct ions of the form $[\text{M}+\text{Cl}]^-$, $[\text{M}+\text{NO}_3]^-$, $[\text{M}+\text{I}]^-$, and $[\text{M}+\text{Ac}]^-$, respectively. The relative sensitivities of individual adduct ions increase by ultimately two orders of magnitude, compared with the pure standard in methanol solution. Here the observed ion adduct formation in ESI can be considered as a special case of chemical ionization occurring in solution before the charge separation process takes place.

Table 1 lists the characteristic adduct ions formed from three AN standards (MNG, DNG, and PETN) in methanol solution with selected additives (NH_4Ac , NH_4Cl , NaI , and NaNO_3). Ion adducts are systematically observed from all of the ANs investigated, regardless of the number of $-\text{ONO}_2$ functional groups attached on the molecule. Nitrate (NO_3^-) and chloride (Cl^-) anions were found to be the most effective additives to promote ion adduct formation. Nitrate clusters exhibit the highest signal intensity and lowest limit of detection, especially for the poly-nitrates and functionalized alkyl nitrates investigated. Chloride clusters are characterized by two distinct ions with a mass difference of 2 amu and abundance ratio of 3:1 due to the natural presence of isotopes ^{35}Cl and ^{37}Cl . Also given in Table 1 are the detected negative ions from two organic nitro compounds, i.e., hexahydro-1,3,5-trinitro-1,3,5-triazine (RDX) and 2,4-dinitrotoluene (DNT). In contrast to RDX, which undergoes intensive clustering processes with Cl^- , I^- ,

and NO_3^- during negative ESI, one dominant molecular ion ($[\text{M-H}]^-$) was observed on the ESI(−) mass spectra of DNT. The limits of detection (LOD) towards the nitrate adducts are in the range of 0.1 to 4.3 μM (see Table 1), demonstrating an improved performance of the IMS-MS technique employed here compared with literature data obtained from sprayed solutions (Asbury et al., 2000; Hilton et al., 2010). For example, the LODs for DNT and RDX are 26 $\mu\text{g/L}$ and 40 $\mu\text{g/L}$, respectively, in Asbury et al. (2000), and the LOD for urea nitrate is 2.5 mg/L in Hilton et al. (2010).

The effect of the additive concentrations (NO_3^- and Cl^-) on the ion adduct formation was investigated using an equimolar mixture (5 μM each) of PETN and RDX as representative of nitrates and nitro compounds, respectively, in methanol solution (Figure 2). In the absence of any additives, the presence of background anions from either impurities in the solvent or thermal decomposition of alkyl nitrates leads to a detectable amount of ion adducts. With the anion levels on the order of micromolar, ion adducts become dominant in the ESI(−) mass spectra. The optimal anion concentration was found to be in the range of 0.01 mM to 0.1 mM. Progressively rising anion concentrations ($> 1\text{mM}$) essentially suppress adduct formation due to the competition for limited resources, such as space and charge (Cech and Enke, 2001). Note that the measured drift time for each ion adduct is constant at anion concentrations ranging from 1 μM to 1 mM, indicative of the absence of ion-molecule clustering in the IMS drift tube.

3.2. Collision cross section vs. mass to charge ratio trend line

Collision cross section (Ω_{N_2}) represents the effective area for interactions between a charged molecule and the surrounding buffer gases (e.g., N_2 herein). It is derived from the mobility measurement in the IMS drift tube, where ions with open conformation undergo more collisions with buffer gas molecules and hence travel more slowly than the compact ones (Shvartsburg et al., 2000). The measured Ω_{N_2} for organic nitrates and nitro compounds given in Table 1 are in good agreement with previous reported values obtained from experiments where the analytes were introduced into the IMS system from the vapor phase (Kaur-Atwal et al., 2009; Kozole et al., 2015). Combination of collision cross section with molecular mass (as denoted by mass to charge ratio, m/z) provides a two-dimensional space for separation of species based on their size as well as geometry. We have shown that species of the same chemical class (e.g., amines, alcohols, and carboxylic acids) tend to situate as a narrow band and follow a unique trend line on the 2-D space (Zhang et al., 2016b). Here we demonstrate the presence of a $\Omega_{\text{N}_2} - m/z$ trend line for alkyl nitrates. Figure 3 shows that the measured Ω_{N_2} of the AN adducts,

regardless of the AN molecular structures and types of anions that promote the adduct formation, appear along the $\Omega_{N_2} - m/z$ trend line predicted by the core model (deviations less than 5.2%). Also shown here are the predicted $\Omega_{N_2} - m/z$ trend lines for *mono/multi*-carboxylic acids and organic sulfates, which readily produce molecular ions via deprotonation ($[M-H]^-$) during negative ESI. Alkyl nitrates can be distinguished from carboxylic acids and sulfates based on their distinct collision cross sections vs. mass to charge ratio relationship. Note that other important chemical classes of atmospheric interest, such as amines, alcohols, aldehydes, and peroxides, are suitable for analysis in the positive ESI and their trend lines are not given here.

3.3. Characteristic fragments upon collision-induced dissociation

Molecular structures of selected AN ion adducts were further probed with the assistance of the collision-induced dissociation (CID) analysis, which was performed after the drift tube but prior to the time-of-flight chamber. The resulting daughter ion appears at the same drift time as the parent ion, allowing for a straightforward correlation of any given ion with its fragments. As shown in Figure 4, the nitrate ion (NO_3^-) at m/z 62 is exclusively observed upon CID of the parent ion adducts formed from MNG, DNG, and PETN by clustering with Cl^- , NO_3^- , and Ac^- . The NO_3^- fragment resulting from decomposition of the corresponding parent ion adduct can be well separated from that originally added to the AN solution based on their entirely different ion mobilities (as reflected by the measured drift time). Thus NO_3^- is considered as a characteristic fragment upon CID of the parent AN adduct ion and serves as a tracer to verify the presence of the $-ONO_2$ functional group in unknown compounds.

The anions (Cl^- , NO_3^- , and Ac^-) that promote the clustering chemistry were not observed upon CID of the parent AN adducts. Figure 5 shows the profiles of four ion adducts, i.e., $[MNG+Cl]^-$, $[MNG+Ac]^-$, $[PETN+Cl]^-$, and $[PETN+I]^-$, as well as their resulting fragments under a sequence of CID potential gradient. As expected, the abundance of the transmitted parent ion adducts decreases as the CID voltage rises. NO_3^- appears as the largest product ion, and its enhanced abundance with increasing CID voltage is balanced by the decrease in signals of the corresponding parent ion adduct. Cl^- and Ac^- remain minor peaks over the entire range of displayed CID potential gradient. Under low-energy collisions, the parent AN ion adduct principally follows two fragmentation pathways, leading to either $Cl^-/Ac^-/I^-$ with the neutral AN molecule or the deprotonated AN molecular ion ($[M-H]^-$) via the neutral loss of HCl / HAc / HI. The absence of Cl^- and Ac^- indicates higher gas-phase basicity of Cl^-/Ac^- than $[M-H]^-$.

As a result, the mechanism yielding $[M-H]^-$ is the dominant fragmentation pathway of AN ion adducts (with an exception for $[PETN+I]^-$). The resulting molecular ion $[M-H]^-$ decomposes promptly to NO_3^- due to the presence of the fragile R-ONO₂ bond.

3.4. Application to isoprene SOA

The OH-initiated oxidation of isoprene produces a population of isoprene peroxy radicals (RO₂), the fate of which depends on the level of nitric oxide. Under high-NO conditions as performed in the chamber experiments here, RO₂ radicals preferentially react with NO leading to major first-generation products including isoprene hydroxy nitrates, among which the two β-hydroxy nitrates dominate the isomer distribution. Due to the presence of a double bond, the hydroxy nitrate could undergo OH addition followed again by reactions of RO₂ radicals with NO, leading to a spectrum of products, of which some highly functionalized molecules such as the dihydroxy dinitrate are potential SOA precursors (Wennberg et al., 2018).

A pair of ion adducts at m/z 261 ($[M+^{35}Cl]^-$) and m/z 263 ($[M+^{37}Cl]^-$) with the abundance ratio of 3:1 is observed in the mass spectra of the isoprene SOA extracts in methanol with 0.2 mM sodium chloride as the additive. These two adducts share an identical mobility (DT = ~25.8 ms), which also appears as a small peak (DT = ~25.7 ms) in the mobility spectra of the NO_3^- ion (bottom panel of Figure 6). Further inspection of the ‘mobility-selected’ mass spectra of the parent ion adduct at m/z 261 reveals that NO_3^- is the major fragment ion (top panel of Figure 6). With the application of a CID potential sequence, the intensity of the precursor ion at m/z 261 decreases and that of the fragment ion at m/z 62 increases (middle panel of Figure 6), a similar pattern observed for the AN standards. We thereby tentatively assign the parent ion adduct at m/z 261 to a second-generation oxidation product, dihydroxy dinitrate (C₅H₁₀O₈N₂, see the chemical structure given in Figure 6), which is produced from the addition of OH to the two double bonds of isoprene followed by RO₂+NO reactions. It is interesting to note that a small shoulder peak appears at ~26.0 ms in the mobility spectra of the ion adduct at m/z 261 (bottom panel of Figure 6), likely representative of the C₅H₁₀O₈N₂ isomers generated from the much less favored OH-addition channels that produce primary RO₂ radicals. Quantitative analysis of the dihydroxy dinitrate is complicated by the matrix interference during the ESI process and chromatographic separation prior to infusion to the ESI source is required (Zhang et al., 2015a; Zhang et al., 2016a), which is beyond the capability of the current instrument setup. Further note that first-generation hydroxy nitrates were not detected, due to their relatively high volatility and thus quite limited partitioning onto the particle phase. On the other hand, multiple peaks were observed in the mobility spectra of

the NO_3^- ion (bottom panel of Figure 6), and their drift times are higher than that of the ion assigned to the dihydroxy dinitrate, implying that some high-molecular-weight nitrate products were likely fragmented in the quadrupole interface.

4. Conclusions

The anion attachment chemistry was previously used in the negative ESI operation to effectively induce ion formation from neutral molecules that lack acidic sites (Zhu and Cole, 2000). Here we build upon the use of anion attachment, a special chemical ionization mechanism in solution, to characterize the condensed-phase alkyl nitrates at molecular level. The propensity of the $-\text{ONO}_2$ moiety to cluster with a diverse selection of anions, including Cl^- , I^- , NO_3^- , and Ac^- , was observed during the negative electrospray ionization process, and the measured total ion signals were enhanced by ultimately two orders of magnitude. Compared with conventional mass spectrometric techniques, the coupled ion mobility and mass-to-charge ratio measurements provide a two-dimensional separation of alkyl nitrates from other chemical classes commonly detected in negative ESI, such as organic sulfates and carboxylic acids. With the assistance of the collision-induced dissociation analysis, upon which the resulting product ions share the identical drift time as the precursor ion, molecular structures of ANs can be further probed. Regardless of the types of anions attached to the AN molecules, dissociation of the parent adduct ion yields a characteristic fragment, NO_3^- at m/z 62, which can be used to verify the presence of the $-\text{ONO}_2$ functional group in any given molecule. These new features enable the unambiguous identification of alkyl nitrates in a complex organic mixture, as exemplified by the detection of hydroxynitrates in isoprene derived SOA. The IMS-MS technique for the measurement of condensed-phase ANs is in its early stages of development. Accurate quantification of a given AN molecule by minimizing the ion suppression and improving the long-term stability of ESI is needed for future work.

Acknowledgements

The National Center for Atmospheric Research is operated by the University Corporation for Atmospheric Research, under the sponsorship of the National Science Foundation.

References

Asbury, G. R., Klasmeier, J., and Hill Jr, H. H.: Analysis of explosives using electrospray ionization/ion mobility spectrometry (ESI/IMS), *Talanta*, 50, 1291-1298, 2000.

335 Atlas, E.: Evidence for \geq C3 alkyl nitrates in rural and remote atmospheres, *Nature*, 331,
 336 426 - 428, 1988.

337 Beaver, M. R., St Clair, J. M., Paulot, F., Spencer, K. M., Crounse, J. D., LaFranchi, B.
 338 W., Min, K. E., Pusede, S. E., Wooldridge, P. J., and Schade, G. W.: Importance of
 339 biogenic precursors to the budget of organic nitrates: observations of multifunctional
 340 organic nitrates by CIMS and TD-LIF during BEARPEX 2009, *Atmos. Chem. Phys.*, 12,
 341 5773-5785, 2012.

342 Brown, S. S., Degouw, J. A., Warneke, C., Ryerson, T. B., Dubé, W. P., Atlas, E.,
 343 Weber, R. J., Peltier, R. E., Neuman, J. A., and Roberts, J. M.: Nocturnal isoprene
 344 oxidation over the Northeast United States in summer and its impact on reactive nitrogen
 345 partitioning and secondary organic aerosol, *Atmos. Chem. Phys.*, 9, 3027-3042, 2009.

346 Cappa, C. D., Zhang, X., Loza, C. L., Craven, J. S., Lee, Y. D., and Seinfeld, J. H.:
 347 Application of the statistical oxidation model (SOM) to secondary organic aerosol
 348 formation from photooxidation of C12 alkanes, *Atmos. Chem. Phys.*, 13, 1591-1606,
 349 2013.

350 Cech, N. B., and Enke, C. G.: Practical implications of some recent studies in
 351 electrospray ionization fundamentals, *Mass Spectrom. Rev.*, 20, 362-387, 2001.

352 Cotte-Rodríguez, I., Takáts, Z., Talaty, N., Chen, H., and Cooks, R. G.: Desorption
 353 electrospray ionization of explosives on surfaces: sensitivity and selectivity enhancement
 354 by reactive desorption electrospray ionization, *Anal. Chem.*, 77, 6755-6764, 2005.

355 Crawford, C. L., and Hill, H. H.: Comparison of reactant and analyte ions for ^{63}Ni nickel,
 356 corona discharge, and secondary electrospray ionization sources with ion mobility-mass
 357 spectrometry, *Talanta*, 107, 225-232, 2013.

358 Day, D. A., Wooldridge, P. J., Dillon, M. B., Thornton, J. A., and Cohen, R. C.: A
 359 thermal dissociation laser - induced fluorescence instrument for in situ detection of NO₂,
 360 peroxy nitrates, alkyl nitrates, and HNO₃, *J. Geophys. Res. Atmos.*, 107, 2002.

361 Farmer, D. K., Matsunaga, A., Docherty, K. S., Surratt, J. D., Seinfeld, J. H., Ziemann, P.
 362 J., and Jimenez, J. L.: Response of an aerosol mass spectrometer to organonitrates and
 363 organosulfates and implications for atmospheric chemistry, *Proc. Natl. Acad. Sci. USA*,
 364 107, 6670-6675, 2010.

365 Farmer, D. K., Perring, A. E., Wooldridge, P. J., Blake, D. R., Baker, A., Meinardi, S.,
 366 Huey, L. G., Tanner, D., Vargas, O., and Cohen, R. C.: Impact of organic nitrates on
 367 urban ozone production, *Atmos. Chem. Phys.*, 11, 4085-4094, 2011.

368 Groessl, M., Graf, S., and Knochenmuss, R.: High resolution ion mobility-mass
 369 spectrometry for separation and identification of isomeric lipids, *Analyst*, 140, 6904-
 370 6911, 2015.

371 He, S., Chen, Z., and Zhang, X.: Photochemical reactions of methyl and ethyl nitrate: a
 372 dual role for alkyl nitrates in the nitrogen cycle, *Environ. Chem.*, 8, 529-542, 2011.

373 He, S. Z., Chen, Z. M., Zhang, X., Zhao, Y., Huang, D. M., Zhao, J. N., Zhu, T., Hu, M.,
 374 and Zeng, L. M.: Measurement of atmospheric hydrogen peroxide and organic peroxides
 375 in Beijing before and during the 2008 Olympic Games: Chemical and physical factors

376 influencing their concentrations, *J. Geophys. Res. Atmos.*, 115, 10.1029/2009JD013544,
 377 2010.

378 Hilton, C. K., Krueger, C. A., Midey, A. J., Osgood, M., Wu, J., and Wu, C.: Improved
 379 analysis of explosives samples with electrospray ionization-high resolution ion mobility
 380 spectrometry (ESI-HRIMS), *Int. J. Mass Spectrom.*, 298, 64-71, 2010.

381 Huang, D. D., Zhang, X., Dalleska, N. F., Lignell, H., Coggon, M. M., Chan, C. M.,
 382 Flagan, R. C., Seinfeld, J. H., and Chan, C. K.: A note on the effects of inorganic seed
 383 aerosol on the oxidation state of secondary organic aerosol— α - pinene ozonolysis, *J.*
 384 *Geophys. Res. Atmos.*, 121, 12476-12483, 2016.

385 Huang, Y., Zhao, R., Charan, S. M., Kenseth, C. M., Zhang, X., and Seinfeld, J. H.:
 386 Unified theory of vapor-wall mass transport in Teflon-walled environmental chambers,
 387 *Environ. Sci. Technol.*, 52, 2134-2142, 2018.

388 Justes, D. R., Talaty, N., Cotte-Rodriguez, I., and Cooks, R. G.: Detection of explosives
 389 on skin using ambient ionization mass spectrometry, *Chemical communications*, 2142-
 390 2144, 2007.

391 Kaplan, K., Graf, S., Tanner, C., Gonin, M., Fuhrer, K., Knochenmuss, R., Dwivedi, P.,
 392 and Hill Jr, H. H.: Resistive Glass IM-TOFMS, *Anal. Chem.*, 82, 9336-9343, 2010.

393 Kaur-Atwal, G., O'Connor, G., Aksenov, A. A., Bocos-Bintintan, V., Thomas, C. L. P.,
 394 and Creaser, C. S.: Chemical standards for ion mobility spectrometry: a review,
 395 *International Journal for Ion Mobility Spectrometry*, 12, 1-14, 2009.

396 Kiendler-Scharr, A., Mensah, A. A., Friese, E., Topping, D., Nemitz, E., Prevot, A. S. H.,
 397 Äijälä, M., Allan, J., Canonaco, F., and Canagaratna, M.: Ubiquity of organic nitrates
 398 from nighttime chemistry in the European submicron aerosol, *Geophys. Res. Lett.*, 43,
 399 7735-7744, 2016.

400 Kozole, J., Levine, L. A., Tomlinson-Phillips, J., and Stairs, J. R.: Gas phase ion
 401 chemistry of an ion mobility spectrometry based explosive trace detector elucidated by
 402 tandem mass spectrometry, *Talanta*, 140, 10-19, 2015.

403 Krechmer, J. E., Coggon, M. M., Massoli, P., Nguyen, T. B., Crounse, J. D., Hu, W.,
 404 Day, D. A., Tyndall, G. S., Henze, D. K., Rivera-Rios, J. C., Nowak, J. B., Kimmel, J. R.,
 405 III, R. L. M., Stark, H., Jayne, J. T., Sipila, M., Junninen, H., Clair, J. M. S., Zhang, X.,
 406 Feiner, P. A., Zhang, L., Miller, D. O., Brune, W. H., Keutsch, F. N., Wennberg, P. O.,
 407 Seinfeld, J. H., Worsnop, D. R., Jimenez, J. L., and Canagaratna, M. R.: Formation of
 408 low volatility organic compounds and secondary organic aerosol from isoprene
 409 hydroxyhydroperoxide low-NO oxidation, *Environ. Sci. Technol.*, 49, 10330-10339,
 410 2015.

411 Krechmer, J. E., Groessl, M., Zhang, X., Junninen, H., Massoli, P., Lambe, A. T.,
 412 Kimmel, J. R., Cubison, M. J., Graf, S., Lin, Y. H., Budisulistiorini, S. H., Zhang, H.,
 413 Surratt, J. D., Knochenmuss, R., Jayne, J. T., Worsnop, D. R., Jimenez, J. L., and
 414 Canagaratna, M. R.: Ion mobility spectrometry-mass spectrometry (IMS-MS) for on-
 415 and offline analysis of atmospheric gas and aerosol species, *Atmos. Meas. Tech.*, 9,
 416 3245-3262, 2016.

417 Lambe, A., Massoli, P., Zhang, X., Canagaratna, M., Nowak, J., Daube, C., Yan, C., Nie,
 418 W., Onasch, T., Jayne, J., Kolb, C., Davidovits, P., Worsnop, D., and Brune, W.:
 419 Controlled nitric oxide production via O(1D) + N₂O reactions for use in oxidation flow
 420 reactor studies, *Atmos. Meas. Tech.*, 10, 2283-2298, 2017.

421 Lee, B. H., Mohr, C., Lopez-Hilfiker, F. D., Lutz, A., Hallquist, M., Lee, L., Romer, P.,
 422 Cohen, R. C., Iyer, S., and Kurtén, T.: Highly functionalized organic nitrates in the
 423 southeast United States: Contribution to secondary organic aerosol and reactive nitrogen
 424 budgets, *Proc. Natl. Acad. Sci. USA*, 113, 1516-1521, 2016.

425 Loza, C. L., Craven, J. S., Yee, L. D., Coggon, M. M., Schwantes, R. H., Shiraiwa, M.,
 426 Zhang, X., Schilling, K. A., Ng, N. L., and Canagaratna, M. R.: Secondary organic
 427 aerosol yields of 12-carbon alkanes, *Atmos. Chem. Phys.*, 14, 1423-1439, 2014.

428 Martínez-Lozano, P., Rus, J., de la Mora, G. F., Hernández, M., and de la Mora, J. F.:
 429 Secondary electrospray ionization (SESI) of ambient vapors for explosive detection at
 430 concentrations below parts per trillion, *J. Am. Soc. Mass Spectrom.*, 20, 287-294, 2009.

431 McVay, R. C., Zhang, X., Aumont, B., Valorso, R., Camredon, M., La, Y. S., Wennberg,
 432 P. O., and Seinfeld, J. H.: SOA formation from the photooxidation of α -pinene:
 433 systematic exploration of the simulation of chamber data, *Atmos. Chem. Phys.*, 16, 2785-
 434 2802, 2016.

435 Nah, T., McVay, R. C., Zhang, X., Boyd, C. M., Seinfeld, J. H., and Ng, N. L.: Influence
 436 of seed aerosol surface area and oxidation rate on vapor wall deposition and SOA mass
 437 yields: a case study with α -pinene ozonolysis, *Atmos. Chem. Phys.*, 16, 9361-9379,
 438 2016.

439 Nguyen, T. B., Coggon, M. M., Bates, K. H., Zhang, X., Schwantes, R. H., Schilling, K.
 440 A., Loza, C. L., Flagan, R. C., Wennberg, P. O., and Seinfeld, J. H.: Organic aerosol
 441 formation from the reactive uptake of isoprene epoxydiols (IEPOX) onto non-acidified
 442 inorganic seeds, *Atmos. Chem. Phys.*, 14, 3497-3510, 2014a.

443 Nguyen, T. B., Crounse, J. D., Schwantes, R. H., Teng, A. P., Bates, K. H., Zhang, X., St
 444 Clair, J. M., Brune, W. H., Tyndall, G. S., and Keutsch, F. N.: Overview of the Focused
 445 Isoprene eXperiment at the California Institute of Technology (FIXCIT): mechanistic
 446 chamber studies on the oxidation of biogenic compounds, *Atmos. Chem. Phys.*, 14,
 447 13531-13549, 2014b.

448 Nguyen, T. B., Bates, K. H., Crounse, J. D., Schwantes, R. H., Zhang, X., Kjaergaard, H.
 449 G., Surratt, J. D., Lin, P., Laskin, A., and Seinfeld, J. H.: Mechanism of the hydroxyl
 450 radical oxidation of methacryloyl peroxyxynitrate (MPAN) and its pathway toward
 451 secondary organic aerosol formation in the atmosphere, *Phys. Chem. Chem. Phys.*, 17,
 452 17914-17926, 2015.

453 O'Brien, J. M., Shepson, P. B., Muthuramu, K., Hao, C., Niki, H., Hastie, D. R., Taylor,
 454 R., and Roussel, P. B.: Measurements of alkyl and multifunctional organic nitrates at a
 455 rural site in Ontario, *J. Geophys. Res. Atmos.*, 100, 22795-22804, 1995.

456 Perring, A. E., Pusede, S. E., and Cohen, R. C.: An observational perspective on the
 457 atmospheric impacts of alkyl and multifunctional nitrates on ozone and secondary
 458 organic aerosol, *Chem. Rev.*, 113, 5848-5870, 2013.

459 Popov, I. A., Chen, H., Kharybin, O. N., Nikolaev, E. N., and Cooks, R. G.: Detection of
 460 explosives on solid surfaces by thermal desorption and ambient ion/molecule reactions,
 461 Chemical Communications, 1953-1955, 2005.

462 Riva, M., Budisulistiorini, S. H., Chen, Y., Zhang, Z., D'Ambro, E. L., Zhang, X., Gold,
 463 A., Turpin, B. J., Thornton, J. A., and Canagaratna, M. R.: Chemical characterization of
 464 secondary organic aerosol from oxidation of isoprene hydroxyhydroperoxides, Environ.
 465 Sci. Technol., 50, 9889-9899, 2016.

466 Rollins, A. W., Smith, J. D., Wilson, K. R., and Cohen, R. C.: Real time in situ detection
 467 of organic nitrates in atmospheric aerosols, Environ. Sci. Technol., 44, 5540-5545, 2010.

468 Rollins, A. W., Browne, E. C., Min, K. E., Pusede, S. E., Wooldridge, P. J., Gentner, D.
 469 R., Goldstein, A. H., Liu, S., Day, D. A., and Russell, L. M.: Evidence for NO_x control
 470 over nighttime SOA formation, Science, 337, 1210-1212, 2012.

471 Rosen, R. S., Wood, E. C., Wooldridge, P. J., Thornton, J. A., Day, D. A., Kuster, W.,
 472 Williams, E. J., Jobson, B. T., and Cohen, R. C.: Observations of total alkyl nitrates
 473 during Texas Air Quality Study 2000: Implications for O₃ and alkyl nitrate
 474 photochemistry, J. Geophys. Res. Atmos., 109, 2004.

475 Russell, L. M., Bahadur, R., and Ziemann, P. J.: Identifying organic aerosol sources by
 476 comparing functional group composition in chamber and atmospheric particles, Proc.
 477 Natl. Acad. Sci. USA, 108, 3516-3521, 2011.

478 Schilling Fahnestock, K. A., Yee, L. D., Loza, C. L., Coggon, M. M., Schwantes, R.,
 479 Zhang, X., Dalleska, N. F., and Seinfeld, J. H.: Secondary organic aerosol composition
 480 from C₁₂ alkanes, J. Phys. Chem. A, 119, 4281-4297, 2014.

481 Schwantes, R. H., Teng, A. P., Nguyen, T. B., Coggon, M. M., Crounse, J. D., St. Clair,
 482 J. M., Zhang, X., Schilling, K. A., Seinfeld, J. H., and Wennberg, P. O.: Isoprene NO₃
 483 Oxidation Products from the RO₂+ HO₂ Pathway, J. Phys. Chem. A, 119, 10158-10171,
 484 2015.

485 Schwantes, R. H., McVay, R. C., Zhang, X., Coggon, M. M., Lignell, H., Flagan, R. C.,
 486 Wennberg, P. O., and Seinfeld, J. H.: Science of the environmental chamber, Advances in
 487 Atmospheric Chemistry, 1, 1-93, 2017a.

488 Schwantes, R. H., Schilling, K. A., McVay, R. C., Lignell, H., Coggon, M. M., Zhang,
 489 X., Wennberg, P. O., and Seinfeld, J. H.: Formation of highly oxygenated low-volatility
 490 products from cresol oxidation, Atmos. Chem. Phys., 17, 3453-3474, 2017b.

491 Shvartsburg, A. A., Liu, B., Jarrold, M. F., and Ho, K.-M.: Modeling ionic mobilities by
 492 scattering on electronic density isosurfaces: Application to silicon cluster anions, J.
 493 Chem. Phys., 112, 4517-4526, 2000.

494 Takáts, Z., Cotte-Rodriguez, I., Talaty, N., Chen, H., and Cooks, R. G.: Direct, trace level
 495 detection of explosives on ambient surfaces by desorption electrospray ionization mass
 496 spectrometry, Chemical Communications, 1950-1952, 2005.

497 Tam, M., and Hill, H. H.: Secondary electrospray ionization-ion mobility spectrometry
 498 for explosive vapor detection, Anal. Chem., 76, 2741-2747, 2004.

499 Teng, A. P., Crounse, J. D., Lee, L., St Clair, J. M., Cohen, R. C., and Wennberg, P. O.:
 500 Hydroxy nitrate production in the OH-initiated oxidation of alkenes, *Atmos. Chem.*
 501 *Phys.*, 15, 4297-4316, 2015.

502 Thomas, D. A., Coggon, M. M., Lignell, H., Schilling, K. A., Zhang, X., Schwantes, R.
 503 H., Flagan, R. C., Seinfeld, J. H., and Beauchamp, J. L.: Real-time studies of iron
 504 oxalate-mediated oxidation of glycolaldehyde as a model for photochemical aging of
 505 aqueous tropospheric aerosols, *Environ. Sci. Technol.*, 50, 12241-12249, 2016.

506 Thornton, J. A., Wooldridge, P. J., and Cohen, R. C.: Atmospheric NO₂: In situ laser-
 507 induced fluorescence detection at parts per trillion mixing ratios, *Anal. Chem.*, 72, 528-
 508 539, 2000.

509 Wang, H., Zhang, X., and Chen, Z.: Development of DNPH/HPLC method for the
 510 measurement of carbonyl compounds in the aqueous phase: applications to laboratory
 511 simulation and field measurement, *Environ. Chem.*, 6, 389-397, 2009.

512 Wennberg, P. O., Bates, K. H., Crounse, J. D., Dodson, L. G., McVay, R. C., Mertens, L.
 513 A., Nguyen, T. B., Praske, E., Schwantes, R. H., and Smarte, M. D.: Gas-phase reactions
 514 of isoprene and its major oxidation products, *Chem. Rev.*, 118, 3337-3390, 2018.

515 Wooldridge, P. J., Perring, A. E., Bertram, T. H., Flocke, F. M., Roberts, J. M., Singh, H.
 516 B., Huey, L. G., Thornton, J. A., Wolfe, G. M., and Murphy, J. G.: Total Peroxy Nitrates
 517 (Σ PNs) in the atmosphere: the Thermal Dissociation-Laser Induced Fluorescence (TD-
 518 LIF) technique and comparisons to speciated PAN measurements, *Atmos. Meas. Tech.*,
 519 3, 593-607, 2010.

520 Xiong, F., McAvey, K. M., Pratt, K. A., Groff, C. J., Hostetler, M. A., Lipton, M. A.,
 521 Starn, T. K., Seeley, J. V., Bertman, S. B., and Teng, A. P.: Observation of isoprene
 522 hydroxynitrates in the southeastern United States and implications for the fate of NO_x,
 523 *Atmos. Chem. Phys.*, 15, 11257-11272, 2015.

524 Xu, W., Croteau, P., Williams, L., Canagaratna, M., Onasch, T., Cross, E., Zhang, X.,
 525 Robinson, W., Worsnop, D., and Jayne, J.: Laboratory characterization of an aerosol
 526 chemical speciation monitor with PM_{2.5} measurement capability, *Aerosol Sci. Tech.*,
 527 51, 69-83, 2017.

528 Xu, W., Lambe, A., Silva, P., Hu, W., Onasch, T., Williams, L., Croteau, P., Zhang, X.,
 529 Renbaum-Wolff, L., and Fortner, E.: Laboratory evaluation of species-dependent relative
 530 ionization efficiencies in the Aerodyne Aerosol Mass Spectrometer, *Aerosol Sci. Tech.*,
 531 52, 626-641, 2018.

532 Zhang, X., and Seinfeld, J. H.: A functional group oxidation model (FGOM) for SOA
 533 formation and aging, *Atmos. Chem. Phys.*, 13, 5907-5926, 2013.

534 Zhang, X., Cappa, C. D., Jathar, S. H., McVay, R. C., Ensberg, J. J., Kleeman, M. J., and
 535 Seinfeld, J. H.: Influence of vapor wall loss in laboratory chambers on yields of
 536 secondary organic aerosol, *Proc. Natl. Acad. Sci. USA*, 111, 5802-5807, 2014a.

537 Zhang, X., Schwantes, R. H., Coggon, M. M., Loza, C. L., Schilling, K. A., Flagan, R.
 538 C., and Seinfeld, J. H.: Role of ozone in SOA formation from alkane photooxidation,
 539 *Atmos. Chem. Phys.*, 14, 1733-1753, 2014b.

540 Zhang, X., McVay, R. C., Huang, D. D., Dalleska, N. F., Aumont, B., Flagan, R. C., and
 541 Seinfeld, J. H.: Formation and evolution of molecular products in α -pinene secondary
 542 organic aerosol, *Proc. Natl. Acad. Sci. USA*, 112, 14168-14173, 2015a.

	Compound	Molecular	Ion	LOD ^a	Ω_{N_2} ^b	Structure
543	Zhang, X., Schwantes, R. H., McVay, R. C., Lignell, H., Coggon, M. M., Flagan, R. C.,					
544	and Seinfeld, J. H.: Vapor wall deposition in Teflon chambers, <i>Atmos. Chem. Phys.</i> , 15,					
545	4197-4214, 2015b.					
546	Zhang, X., Dalleska, N. F., Huang, D. D., Bates, K. H., Sorooshian, A., Flagan, R. C.,					
547	and Seinfeld, J. H.: Time-resolved molecular characterization of organic aerosols by					
548	PILS+ UPLC/ESI-Q-TOFMS, <i>Atmos. Environ.</i> , 130, 180-189, 2016a.					
549	Zhang, X., Krechmer, J. E., Groessl, M., Xu, W., Graf, S., Cubison, M., Jayne, J. T.,					
550	Jimenez, J. L., Worsnop, D. R., and Canagaratna, M. R.: A novel framework for					
551	molecular characterization of atmospherically relevant organic compounds based on					
552	collision cross section and mass-to-charge ratio, <i>Atmos. Chem. Phys.</i> , 16, 12945-12959,					
553	2016b.					
554	Zhang, X., Lambe, A. T., Upshur, M. A., Brooks, W. A., Gray Bé, A., Thomson, R. J.,					
555	Geiger, F. M., Surratt, J. D., Zhang, Z., and Gold, A.: Highly oxygenated multifunctional					
556	compounds in α -pinene secondary organic aerosol, <i>Environ. Sci. Technol.</i> , 51, 5932-					
557	5940, 2017.					
558	Zhang, X., Ortega, J., Huang, Y., Shertz, S., Tyndall, G. S., and Orlando, J. J.: A steady-					
559	state continuous flow chamber for the study of daytime and nighttime chemistry under					
560	atmospherically relevant NO levels, <i>Atmos. Meas. Tech.</i> , 11, 2537-2551, 2018.					
561	Zhao, Y., Chen, Z., Shen, X., and Zhang, X.: Kinetics and mechanisms of heterogeneous					
562	reaction of gaseous hydrogen peroxide on mineral oxide particles, <i>Environ. Sci. Technol.</i> ,					
563	45, 3317-3324, 2011.					
564	Zhu, J., and Cole, R. B.: Formation and decompositions of chloride adduct ions, $[M+$					
565	$Cl]^-$, in negative ion electrospray ionization mass spectrometry, <i>J. Am. Soc. Mass</i>					
566	<i>Spectrom.</i> , 11, 932-941, 2000.					

567

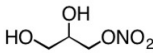
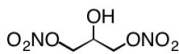
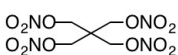
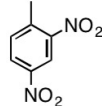
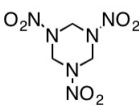
568

569

570

571

572 Table 1. Overview of compounds containing $-ONO_2$ and $-NO_2$ functional groups
 573 investigated in this study.

	Formula	Formula	m/z	(μM)	(\AA^2)	
1-Mononitroglycerin (MNG)	$\text{C}_3\text{H}_7\text{NO}_5$	$[\text{M}+\text{Cl}]^-$	172.0	0.8	129.4	
		$[\text{M}+\text{NO}_2-\text{H}]^-$	182.0	0.7	132.7	
		$[\text{M}+\text{Ac}]^-$	196.0	0.3	139.2	
1,3-Dinitroglycerin (DNG)	$\text{C}_3\text{H}_6\text{N}_2\text{O}_7$	$[\text{M}+\text{Cl}]^-$	217.0	1.1	151.1	
		$[\text{M}+\text{NO}_2-\text{H}]^-$	227.0	4.3	156.6	
		$[\text{M}+\text{NO}_3]^-$	244.0	0.6	151.7	
		$[\text{M}+\text{I}]^-$	308.9	0.8	177.0	
Pentaerythritol tetranitrate (PETN)	$\text{C}_5\text{H}_8\text{N}_4\text{O}_{12}$	$[\text{M}-\text{H}]^-$	315.0	1.1	181.7	
		$[\text{M}+\text{Cl}]^-$	351.0	0.5	183.7	
		$[\text{M}+\text{NO}_2-\text{H}]^-$	361.0	0.9	190.7	
		$[\text{M}+\text{NO}_3]^-$	378.0	0.2	190.9	
		$[\text{M}+\text{I}]^-$	442.9	0.1	216.2	
		$[2\text{M}+\text{Cl}]^-$	667.0	1.0	262.6	
2,4-Dinitrotoluene (DNT)	$\text{C}_7\text{H}_6\text{N}_2\text{O}_4$	$[\text{M}-\text{H}]^-$	181.0	0.6	137.0	
Hexahydro-1,3,5- trinitro-1,3,5-triazine (RDX)	$\text{C}_3\text{H}_6\text{N}_6\text{O}_6$	$[\text{M}+\text{Cl}]^-$	257.0	0.3	149.8	
		$[\text{M}+\text{NO}_2-\text{H}]^-$	267.1	1.4	156.3	
		$[\text{M}+\text{NO}_3]^-$	284.0	0.2	160.8	
		$[\text{M}+\text{I}]^-$	348.9	0.1	181.9	
		$[2\text{M}+\text{Cl}]^-$	479.0	1.6	203.5	

^a The limit of detection (LOD) is calculated as $\text{LOD} = \sigma \times (\text{S/N})/k$, where S/N is the signal-to-noise ratio, which is taken as 3 here, k is the response factor of IMS-MS towards individual ion adducts produced from 5 μM standard nitrate solution during negative ESI, and σ is the standard deviation of the IMS-MS response over the course of 60 s measurements.

^b The collision cross section (Ω_{N_2}) is calculated through the modified zero field (so called Mason-Schamp) equation, see more details in Zhang et al. (2016).

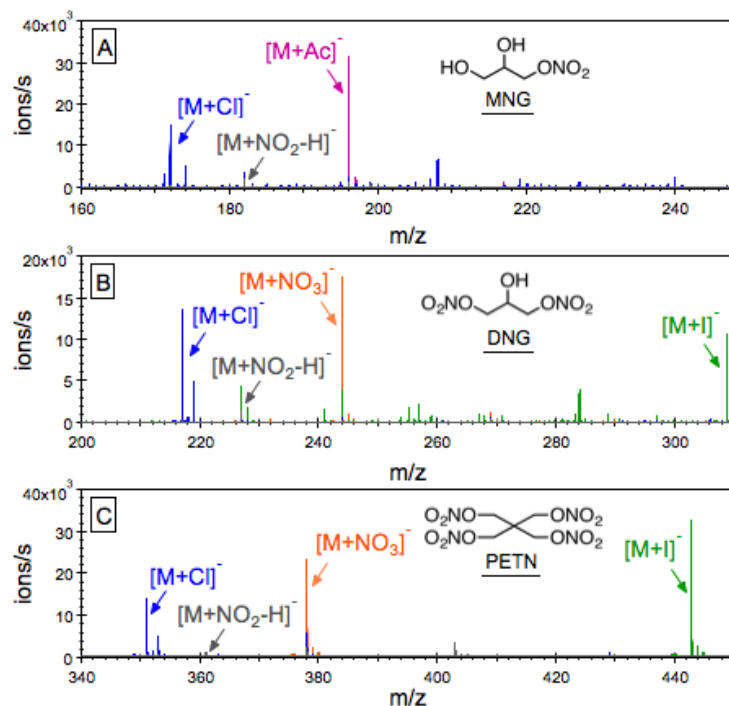


Figure 1. Negative ESI mass spectra of 5 μ M 1-mononitroglycerin (MNG), 1,3-dinitroglycerin (DNG), and pentaerythritol tetranitrate (PETN) dissolved in pure methanol (gray), methanol with 0.1 mM ammonium acetate (NH_4Ac , purple), methanol with 0.1 mM ammonium chloride (NH_4Cl , blue), methanol with 0.1 mM sodium nitrate ($NaNO_3$, orange), and methanol with 0.1 mM sodium iodide (NaI , green). These three alkyl nitrates, which do not readily produce significant amount of molecular ions on their own during negative ESI, are observed as clusters with acetate (Ac^-), chloride (Cl^-), nitrate (NO_3^-), and iodide anions (I^-) in the ESI(-) spectra.

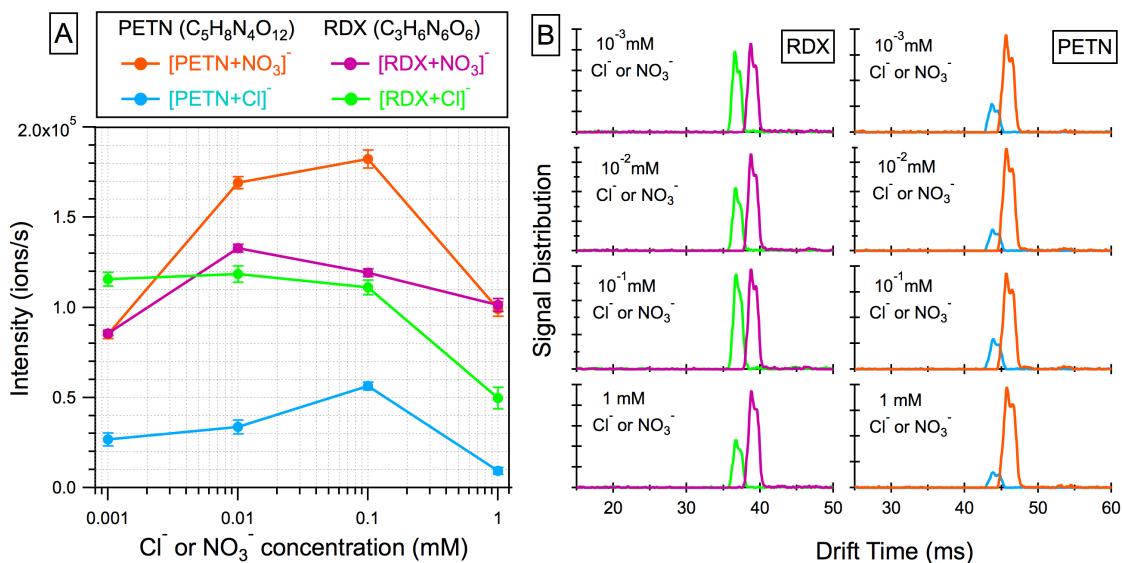
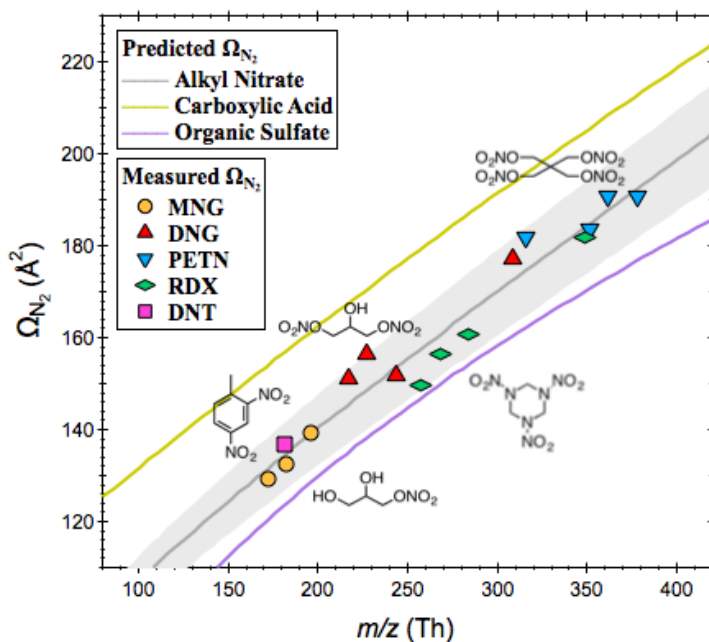


Figure 2. (A) Signals of the ion adducts produced from RDX and PETN by clustering with chloride (Cl^-) and nitrate (NO_3^-) as a function of the corresponding anion concentrations ranging from 1 μM to 1 mM. (B) Drift time distributions of the ion adducts $[\text{RDX}+\text{Cl}]^-$, $[\text{PETN}+\text{Cl}]^-$, $[\text{RDX}+\text{NO}_3]^-$, and $[\text{PETN}+\text{NO}_3]^-$ are consistent at different anion concentrations.



607

608

Figure 3. Measured collision cross sections (Ω_{N_2}) of the AN ion adducts as a function of their mass-to-charge ratios appear along the predicted $\Omega_{N_2} - m/z$ trend line. Also shown here are the predicted $\Omega_{N_2} - m/z$ trend lines for carboxylic acids and organic sulfates, which are major chemical classes of atmospheric interest detected in the negative ESI mode.

614

615

616

617

618

619

620

621

622

623

624

625

626

627

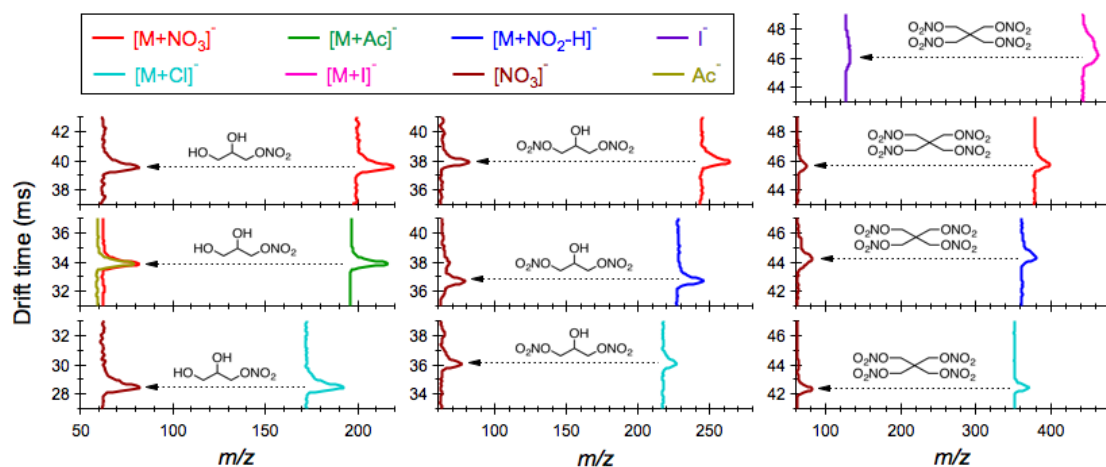
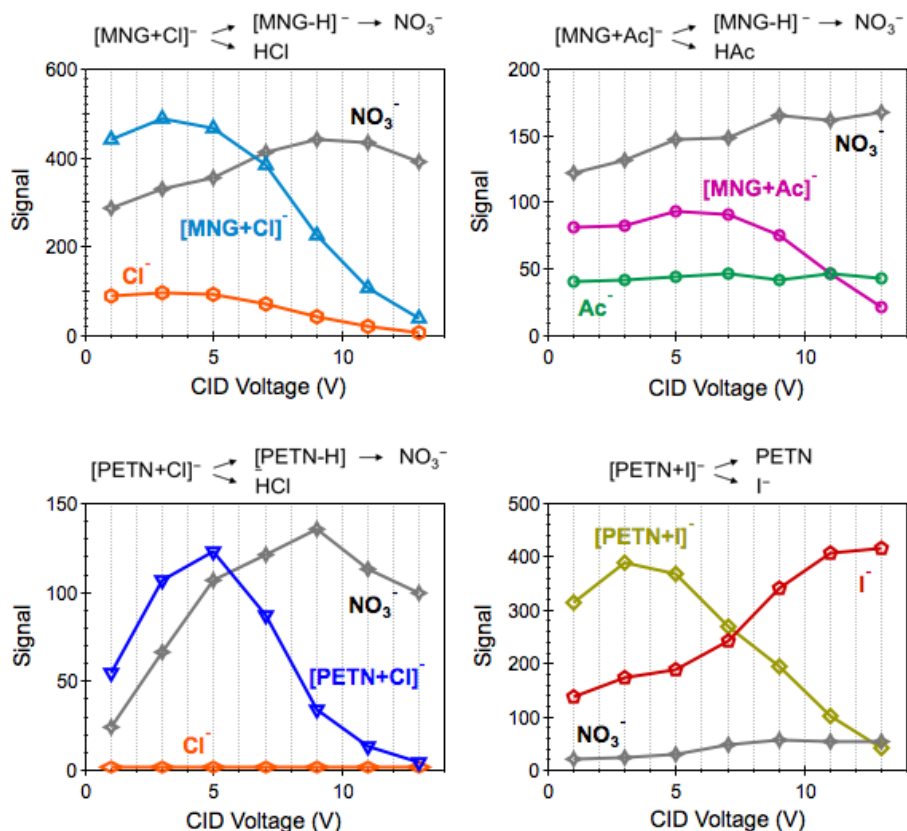


Figure 4. Characteristic fragment ions produced from MNG, DNG, and PETN by clustering with acetate (Ac^-), chloride (Cl^-), iodide (I^-), nitrate (NO_3^-), and nitrite (NO_2^-) upon collision induced dissociation performed at a CID voltage of 20 V.

656



657

658

659 Figure 5. Peak intensities of the precursor ion adducts $[MNG+Cl]^-$, $[MNG+Ac]^-$,
 660 $[PETN+Cl]^-$, and $[PETN+I]^-$ as well as their fragment ions as a function of the collision
 661 energy as displayed by the CID voltage.

662

663

664

665

666

667

668

669

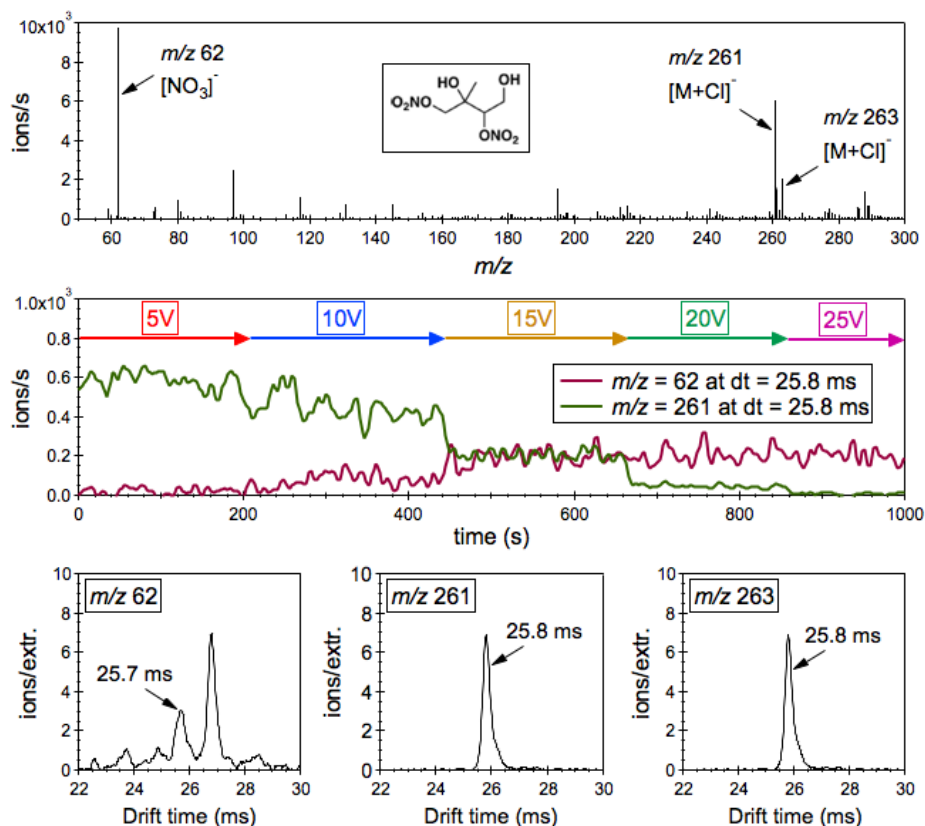


Figure 6. (Top panel) The ‘mobility-selected’ mass spectra of the parent ion adduct at m/z 261 and its major fragment at m/z 62 in isoprene SOA extracts with ~ 0.2 mM sodium chloride as the additive. (Middle panel) Profiles of the precursor ion adduct at m/z 261 and its product ion at m/z 62 as a function of the CID voltage. (Bottom panel) Drift time spectra of the ion adduct at m/z 261, its isotope ion adduct at m/z 263, and the fragment ion at m/z 62.